Real Time Advanced Receiver Autonomous Integrity Monitoring in DLR's Multi-Antenna GNSS Receiver

Markus Rippl, *German Aerospace Center (DLR)*

BIOGRAPHY

Markus Rippl received his Diploma in Electrical Engineering and Information Technology from Technische Universität München (TUM) in 2007. Since then, he has been a research fellow with the Institute of Communications and Navigation (IKN) at the German Aerospace Center (DLR), in Oberpfaffenhofen near Munich. His field of work is the integrity of GNSS-based navigation using receiver-side algorithms.

ABSTRACT

The present paper introduces a real-time implementation of Advanced Receiver Autonomous Integrity Monitoring (ARAIM) implemented in DLR's array antenna receiver "GALANT". The receiver is capable of tracking multiple frequency measurements both from GPS and Galileo signals. The position, velocity and time (PVT) unit and the Multi-Hypothesis Solution Separation (MHSS) based ARAIM unit are closely coupled and operate in a real-time processing environment within the receiver demonstrator.

The presented MHSS based RAIM is extended with Fault Detection and Exclusion (FDE) functionality that can identify large measurement faults in one or multiple range measurements, and adapt its measurement model to mitigate the effects of such biases. Different concepts to obtain such FDE functionality are discussed and compared.

A series of measurements using the Galileo Testbed GATE has been recorded and processed in real time using the presented hardware/software platform. Feared event scenarios were generated by introducing biases to one or multiple pseudorange observations on signal level, i.e. at the GATE processing facility. The PVT and integrity results for nominal and feared event scenarios are presented. The ability of MHSS ARAIM to provide a robust navigation solution in the presence of such large faults is assessed and the improvement of positioning accuracy introduced through the application of FDE methods is demonstrated.

I. INTRODUCTION

ARAIM was introduced in [1], [2] and derived from [3]. It is a RAIM method capable of obtaining navigation integrity for stand-alone users and was designed to exploit the high number and quality of GNSS signals that will be available in the future. As opposed to classical weighted least square RAIM [4] it allows for more stringent integrity requirements like for precision approach of aircraft. The most remarkable improvement is in its ability to bound position errors (i.e. protection levels) under nominal, single or multiple fault conditions. The measurement error model which constitutes the foundation of PL computation is is described as a random variable whose distribution is over bounded by a non centered Gaussian distribution. It is assumed in the whole paper that the ionosphere error is corrected using a dual frequency ionosphere free combination.

It is expected that upon the availability of next-generation GNSS signals from GPS, Galileo, GLONASS and Compass, the worldwide integrity performance using ARAIM will be sufficient to provide LPV-200 navigation capability without the need of conventional augmentation systems such as WAAS or EGNOS [5]. While standardization of ARAIM and the underlying assumptions is in its initial phase [6], [7], it is already conceivable that a large step is made in terms of algorithm complexity by transitioning from slope-based RAIM to ARAIM. Even at the pace of performance increase in today's embedded hardware design, the nature of ARAIM still may limit the feasibility of implementation in avionics in the medium term.

Studies investigating the expected ARAIM performance have been implemented using service volume simulators such as Stanford University's MAAST framework [8], where the user integrity algorithm is directly integrated into a simulation process that generates nominal pseudorange residuals. Functional verification and demonstration of its performance using real data has already been presented in various works [9], [10], [11]. Previous studies apply both current GPS-L1/L2 data from semi-codeless receivers and multi constellation data by the use of GLONASS signals.

The novelty of the present paper is the combination of real GPS and Galileo data, particularly including the analysis of feared event scenarios where ARAIM has to demonstrate its robustness against the threats it was designed for. The generation of such fault scenarios on signal level was accomplished by operating the receiver in the GATE Galileo Testbed [12] in Berchtesgaden, Germany.

Fault Detection and Exclusion (FDE) is the process of identifying large measurement faults and adapt the measurement model of the underlying position estimation process to mitigate the impact of such biases. The multiple hypotheses concept in ARAIM inherently sets the foundation to fault detection capabilities due to the fact that the solution separation determined for each single-fault hypothesis represents the impact

of a single measurement bias on the position estimate. In [13] we presented a novel FDE approach incorporating and extending methods from [9] and [7]. A FDE method based on this suggestion is implemented in the presented real-time receiver platform and validate using feared-event scenarios. It is demonstrated that the ARAIM-FDE is capable of fault identification and mitigation of the bias so that the resulting position error remains at a nominal level, while retaining integrity in terms of a robust vertical protection level (VPL).

A. DLR's Multi-Antenna GNSS Receiver Platform

The GNSS receiver platform presented in this paper was developed at the Institute of Communications and Navigation in the German Aerospace Center (DLR) [14]. The main objectives of the GALANT project were the development of a GNSS receiver capable of receiving data from novel GNSS signals, development of advanced methods for interference and jamming mitigation [15], novel approaches to acquisition and tracking [16], and the use of multiple antenna elements and tracking channels to apply digital beam forming and estimate the Direction-of-Arrival (DoA) for the received signals. After reaching a consequent level of maturity, the GALANT platform became ready to serve as a demonstration platform to implement novel position, velocity and time estimation (PVT), and integrity algorithms.

The GALANT hardware is a 2x2 active antenna array for combined reception of L1 and L5 signals and a corresponding RF front-end for down-conversion and digitalization of the measurements. An FPGA based embedded environment is used for interference countermeasures, acquisition and tracking, and the digital array processing employed to obtain beam steering capabilities using the four antennas. The FPGA board is directly connected to a host PC which serves for tracking loop control, channel control and processing of the derived data from the tracking loops [17]. Here, the pseudorange measurements are extracted from the loop states, and the bit stream containing the navigation data payload is computed. Timestamps are extracted from the navigation data to refer pseudorange observations to system time. Channel control and interaction with the user interface is based in the PC software.

To allow for a modular development of PVT and Integrity modules, the data collected at the receiver software side is encapsulated in an extended set of RTCM3 messages and made available over an Ntrip based network service. Thus, it is possible to connect multiple PVT units to the receiver and process multiple receiver data streams in a single processing environment. Through the use of IP based networking technology, a flexible solution for common laboratory or campaign measurements is possible. In the frame of presented GATE measurements, the receiver PVT and Integrity modules have been executed on a second PC platform connected via Ethernet.

B. Weighted Least Squares Position Estimation

The PVT module can apply carrier smoothing if code and carrier measurements are available simultaneously. However in the presented data, no carrier phases were available and thus, code based pseudoranges have been processed. Because measurements from both E1 and E5 are available, the PVT pre-processing module also supports the generation of Iono-free linear combinations to mitigate the first order ionospheric delay. Due to the high noise level in entirely code-based combinations, this option has not been selected for the presented data. In exchange, the ionospheric delay introduced by the GATE environment has been completely mitigated by application of the same Klobuchar model that was used in the GATE processing facility.

Full decoding of the Galileo I/NAV and F/NAV bitstream is also performed in the PVT module, which allows for a more flexible handling of current and past ephemeris data at instants where the IOD (issue of data) is incremented.

The user position is estimated using a weighted least squares iterative approach. The weighting of the pseudorange measurements needs to be in line with the assumptions used in the MHSS algorithm to compute the Protection Levels. The two modules exchange the weighting coefficients to assure this property.

The combined PVT and ARAIM algorithm uses a NMEA based network output to send its data to a user interface. In order to allow for presentation of ARAIM-specific results in addition to the position estimates, proprietary NMEA sentences have been included with the standardized NMEA datagrams.

II. Advanced Receiver Autonomous Integrity Monitoring with MHSS

The algorithm adopted to guarantee navigation integrity is based on multiple hypothesis[3] technique extended during the past years to MHSS based RAIM [2], [18], [19], with a target to fulfill the integrity requirements for precision approach [20].

ARAIM employs a multiple hypothesis approach to incorporate the potential effects of single or multiple satellite faults into its prediction of the worst case error, the Protection Level (PL). Any combination of faults is first evaluated with respect to its prior probability of occurrence. If a fault mode (i.e., one unique combination of faulted and healthy measurements) is likely to occur, a subset of measurements excluding the potential fault candidates is established and a subset based position is estimated. With all hypothetical position solutions merged into a union of possible positions, the resulting interval is likely to contain a position solution which is based entirely on fault free measurements. The remaining fault hypotheses which were not considered in the interval constitute the set of unmonitored hypotheses, where the sum probability of those is required to be a fraction of the allowable integrity budget applicable to a pre-defined operational mode. For LPV-200 approaches, this integrity risk is defined as $P_{sat} = 1 \cdot 10^{-7}$.

A. Fault model

The model of satellite measurement faults is fundamental to the presented integrity algorithm and is therefore shortly reviewed. First, a satellite measurement is considered to be

present either in a nominal state or in a faulted state. A nominal satellite measurement is described by a measurement fault model including both Gaussian and nominal bias terms. This dual approach is chosen to account both for nominal noise contributions resulting from fast-changing physical error sources such as multipath and receiver noise, and for bias contributions which stem from ephemeris and clock errors, residual ionospheric errors and tropospheric errors. Those biases are assumed to be slowly changing, and typically can be modeled by a nominal magnitude and a maximum magnitude. Both model parameters are applied at different stages of the ARAIM-MHSS algorithm.

The Gaussian part of the measurement error is modeled with the parameters $\sigma_{\text{URE},i}$ and $\sigma_{\text{URA},i}$. The URA-based standard deviation is a Gaussian overbound of the error noise. The bias contribution is described through a nominal parameter b_{nom} and a "nominal maximum" b_{max}.

If the actual measurement error is modeled correctly, the measurement or the satellite is said to be in nominal state. A prior state probability needs to be defined for every satellite used in MHSS in order to compute a tree of hypotheses containing the failure modes and their corresponding probability of occurrence. Here, it is considered that this probability is well known by means of continuous ground monitoring and that the probability data is made available to the user algorithm by an integrity data channel. The underlying architecture to provide such functionality could either be based on GNSS Integrity Channel (GIC) concepts or on concepts pursuing a stand-alone approach for integrity monitoring, discussed under the term Integrity Support Message (ISM) [7]. A probability for constellation wide faults can be applied in a similar way; if constellation wide failures need to be considered, the corresponding hypotheses are established by excluding a complete constellation. Of course, constellation wide faults can only be included in the analysis if measurements from multiple constellations are available, otherwise they are unobservable.

B. Definition of hypotheses

The selection process to determine which fault modes constitute the tree of analyzed hypotheses can be implemented as follows: First, a hypothesis tree combining all possible combination of faults in a set of N visible satellites is constituted. The overall number of hypotheses describing all possible fault combinations including the no-faults hypothesis is the cardinality of the set of hypotheses $\mathfrak{J}$:

$$|\mathfrak{J}| = J = N^2 \tag{1}$$

Assuming statistically independent fault states for individual satellites (this is justifiable if error causes affecting multiple satellites are modeled separately), the fault probability of a single fault mode j with k faulted measurements can be given as

$$P_{ap}(k) = {P_{sat}}^{k} \cdot (1 - P_{sat})^{N-k}, \tag{2}$$

and the total prior probability for all such fault modes with a number of faulted measurements k is

$$\sum_{\text{all } j \text{ with } k \text{ faults}} P_{ap}(k) = \binom{N}{k} \cdot P_{ap}(k). \tag{3}$$

Here, the binomial coefficient $\binom{N}{k}$ has been introduced to define the number of hypotheses that describe modes with k satellite faults. To clearly define the prior probability of a unique failure mode j, we introduce

$$\forall j |\ k \text{ faults}: \quad P_{ap,j} = P_{ap}(k)$$

In a second step, the set of all possible fault modes in $\mathfrak{J}$ is partitioned in the set of hypotheses that are considered in MHSS due to their high probability of occurrence $\mathfrak{J}_{\text{MHSS}}$ and those which are unlikely to be present $\mathfrak{J}_{\text{unknown}}$ and therefore can be neglected in the computation of the VPL.

$$\mathfrak{J} = \mathfrak{J}_{\text{MHSS}} \ \cup \ \mathfrak{J}_{\text{unknown}} \tag{4}$$

The parameter d_{max} defines the maximum number of concurrent satellite faults that need to be considered to establish the MHSS search tree. To determine the maximum search depth all higher order fault mode probabilities are computed starting with the hypothesis excluding all n measurements. Consecutively, hypothesis probabilities corresponding to fewer concurrent faults are added. When a predefined fraction of the admissible integrity budget is taken by the sum of the hypotheses, the loop terminates. When this fault probability fraction has been exceeded and the maximum search depth is fixed, the remaining fault modes constitute the search tree that needs be considered in MHSS. The remaining integrity budget $P_{\text{HMI,MHSS}} = P_{\text{HMI}} - P_{\text{unknown}}$ is recorded to be allocated between those fault modes at a later stage.

A simpler implementation approach considers only single faults and uses a less general error model to estimate the probability of multiple concurrent non-nominal measurement errors. In this case, the integrity budget is simply reduced by a fixed margin allocated to multiple faults, and the remaining budget is split between all one-fault hypotheses and the all-in-view hypothesis.

The requirement of integrity risk needs to account for all fault modes, including those in $\mathfrak{J}_{unknown}$. A conditional probability $P(HMI|j)$ defines the risk of Hazardous Misleading Information (HMI) in case this fault mode applies.

$$P_{HMI} \geq \sum_{j=0}^{J} P_{ap,j} \cdot P(HMI|j) \tag{5}$$

Concerning consummation of integrity budget, the difference between hypotheses in $\mathfrak{J}_{\text{MHSS}}$ and those not under consideration ($\mathfrak{J}_{\text{unknown}}$) is that the prior probability of the latter is directly subtracted from the integrity budget, while hypotheses in the tree only use a fraction of their prior probability in the integrity budget domain. For each hypothesis under investigation the corresponding consummation of integrity budget is the

product of its prior probability and a conditional probability allocation given to the Gaussian overbound used in computing the protection level.

For hypotheses not in the search tree, the conditional probability of HMI, $P(HMI|j) = 1$. The corresponding a priori state probability directly reduces the available integrity budget.

$$\forall j \in \mathfrak{J}_{\text{MHSS}}: \quad P_{\text{HMI},} = P_{ap,j} \cdot P(HMI|j) \tag{6}$$

$$\forall j \in \mathfrak{J}_{\text{unknown}}: \quad P_{\text{HMI},} = P_{ap,j} \tag{7}$$

Consequently, the size of the search tree $\mathfrak{J}_{\text{MHSS}}$ determines the overall use of integrity risk in that considering more fault modes, a smaller fraction of the integrity risk budget needs to be allocated to unknown hypotheses in $\mathfrak{J}_{\text{unknown}}$. In return, more hypotheses with smaller geometries result in higher partial VPLs (Vertical Protection Levels), thus limiting the performance of the algorithm.

C. Computation of hypotheses VPLs

With the definition of a hypothesis tree capable of addressing all fault modes that need consideration within the required integrity budget, a partial VPL for every fault mode can be computed. While the ARAIM flavor currently discussed on international basis [7] only applies geometry based information to determine the VPL and employs measurement data to perform a fault check on the result, the implementation presented here follows [2] and computes a "Real-Time VPL" based on measurements in addition to the predictive VPL. While the prediction VPL stays stationary in case of a satellite fault and is only invalidated by the underlying test, the Real-Time VPL incorporates any position biases caused by such fault and thus inflates when faults are present.

The fundamental philosophy connected with such measurement based error bounds is that it is possible to determine a robust error bound also in the presence of large faults. Whether it is desirable that navigation integrity is still available when the error bound is exceedingly high depends on the use case. For LPV-200, a real-time VPL higher than its prediction but still below the vertical alert limit (VAL) of 35m can still be useful to obtain navigation capability for precision approach. On the other hand, a more conservative approach uses the real-time data just to detect those fault events and disable navigation in such cases.

Both the prediction VPL and the real-time VPL apply a nominal error model based on biases and Gaussian overbounds. The model accounts for any nominal error contributions of the satellite measurements which are hypothetically assumed to be undistorted within the hypothesis. In addition, each partial VPL is increased by a solution separation expression which takes into account the vertical offset of the position estimate that is introduced by exclusion of those satellites that are considered faulty.

In the following developments, the following definitions shall hold: The hypothesis search tree consists of J hypotheses, and j is an index for a single hypothesis. The index 0 corresponds to the all-in-view hypothesis. The size of the all-in-view geometry is N, and n is an index to denote a single measurement.

The solution separation for real-time VPL is obtained from the difference of the vertical all-in-view position solution and the partial solution.

$$d_j = |\Delta x_j - \Delta x_0| \tag{8}$$

Each partial solution is obtained from the pseudorange residuals, projected into the vertical position domain by applying a pseudoinverse specific for the hypothesis, where measurements corresponding to faulted SVs have been canceled:

$$\Delta x_j \quad = \quad \mathbf{h}_v \mathbf{S}_j \Delta \mathbf{y} \tag{9}$$

$$\mathbf{h}_v = [0\ 0\ 1\ 0]$$

$$\mathbf{S}_j = \left(\mathbf{G}^T \mathbf{M}_j \mathbf{W}_{URA} \mathbf{G}\right)^{-1} \mathbf{G}^T \mathbf{M}_j \mathbf{W}_{URA} \tag{10}$$

The pseudoinverse $\mathbf{S}_j$ is derived from the geometry matrix $\mathbf{G}$, the weighting matrix based on the URA error model $\mathbf{W}_{\text{URA}}$ and an identity matrix with zeroed diagonal elements at the position of excluded satellites, $\mathbf{M}_j$. The prediction of the partial VPL estimates a maximum of the fault-free solution separation, employing the probability required for service continuity [7]:

$$D_j = K_{\text{ffd},j} \sigma_{dV,j} + \sum_{n=1}^{N} |\Delta \mathbf{S}_j(3,n)| \cdot b_{\text{nom}} \tag{11}$$

$$\Delta \mathbf{S}_j = \mathbf{S}_j - \mathbf{S}_0 \tag{12}$$

The variance of the Gaussian overbound modeling the vertical solution separation is derived using the nominal variances of the measurement errors (URE) and the nominal bias magnitudes. The tail probability of the Gaussian overbound results from the continuity requirement P_{fa}.

$$\sigma_{dV,j} = \sqrt{\mathbf{dP}_j(3,3)}\ , \text{ where} \tag{13}$$

$$\mathbf{dP}_j = \Delta \mathbf{S}_j {\mathbf{W}_{\text{URE}}}^{-1} \Delta \mathbf{S}_j^T \tag{14}$$

$$K_{\text{ffd},j} = -Q^{-1}\left(\frac{P_{fa}}{2J}\right) \tag{15}$$

Computation of the partial VPLs follows the same approach for both the real-time Protection Level and the prediction

$$\text{VPL}_j = D_j + K_{\text{md},j} \sigma_{V,j} + \sum_{n=1}^{N} |\Delta \mathbf{S}_j(3,n)| \cdot b_{\max}, \tag{16}$$

where the standard deviation of the nominal vertical position error results from

$$\sigma_{V,j} = \sqrt{\mathbf{P}_j(3,3)} \tag{17}$$

$$\mathbf{P}_j = \left(\mathbf{G}^T \mathbf{M}_j \mathbf{W}_{\text{URA}} \mathbf{G}\right)^{-1} \tag{18}$$

The real-time protection level VPL_{RT} applies pseudorange residuals to determine the actual solution separation for the present set of observations. The VPL equation is

$$\text{VPL}_{\text{RT},j} = d_n + K_{\text{md,n}} \sigma_{V,n} + \sum_{i=1}^{N} |\Delta \mathbf{S}_n(3,i)| \cdot b_{\max}. \tag{19}$$

The overall protection levels are derived from the maximum of all corresponding partial VPLs.

$$\text{VPL} = \max_{\text{all } j} \text{VPL}_j \tag{20}$$

$$\text{VPL}_{\text{RT}} = \max_{\text{all } j} \text{VPL}_{\text{RT},j} \tag{21}$$

D. Additional LPV-200 requirements

The LPV-200 precision approach requirements have been established to allow for using SBAS-augmented GNSS navigation for precision approaches down to 200ft vertical visibility. Performance requirements are partially loosened compared to CAT-I, where the vertical alert limit for such navigation is 10m. When LPV-200 is applicable, the vertical requirement for the maximum possible position estimation error is 35m. Since a 35m vertical offset of an airplane at 200ft ceiling can pose significant workload to pilots when the plane arrives above the threshold at too high altitude, a secondary requirement was established to limit the vertical error in fault-free conditions to a 15m. The error bound is called Effective Monitoring Threshold (EMT) and its corresponding integrity risk is required to be below $P_{\text{EMT}} = 10^{-5}$. Another Protection Level requirement at 10m has been introduced [21], [20], and the nominal vertical accuracy is required to be below 4m.

Although previous studies suggest that the EMT requirement is likely to constrain performance even more than the VPL [5], the presented results only analyze the VPL requirement.

E. Fault Detection and Exclusion (FDE)

MHSS based ARAIM can support different methods to detect and identify non-nominal measurement errors. A fundamental principle of ARAIM-based fault detection lies in monitoring the solution separation which is a direct measure of the impact of measurement biases in the observations. Since the solution separation performs a projection of such biases into the vertical position domain, biases detection takes into account each biases significance with respect to the resulting position error.

A fault monitoring approach suggested in [7] compares the solution separation directly with its prediction to determine if one of the excluded measurements has an unusual magnitude:

$$H_{\text{FDE},j} : d_j > D_j \tag{22}$$

This test directly determines if the measurement excluded in H_n corresponds to its model. If a fault is detected, the availability of MHSS based integrity is declined. [7] does not suggest an approach to mitigate such faults and perform exclusion.

Another fault detection approach suggested in [9] is based on an opportunistic attempt to always provide the user with the best possible real-time VPL. It is founded on the assumption that since the real-time implementation of ARAIM uses measurement data instead of a fault model to determine the solution separation it can be trusted to represent the real position error impact of a potential bias in the measurements. If it is assumed that users determines the availability of ARAIM based on the real-time VPL, it is desirable to find a combination of measurements that yield the best possible VPL. In nominal situations, the VPL derived from the all-in-view solution tends to be optimal, because any exclusion of satellites results in degradation of the geometry. If however the exclusion of a satellite excludes a large bias, the corresponding ARAIM VPL based on a reduced geometry does no longer comprise a hypothesis solution separation where this bias is excluded. Thus it is significantly smaller than the all-in-view ARAIM VPL.

However this approach is highly recursive and, without additional tests performed before every epoch, leads to limitations concerning the real-time capability of ARAIM even for state-of-the-art PC based hardware.

A third method combines a-priori exclusion of measurements with a previous test to reduce computational load [13]. Based on the all-in-view MHSS results, it is checked whether

$$\text{VPL}_{\text{RT}} < \text{VPL} \quad , \tag{23}$$

and if the above test fails, a recursive search for smaller real-time VPLs resulting from reduced geometries is started. For every such candidate, it is checked whether the above inequality (23) holds.

Under the assumption that the real-time VPL is robust, it is not necessary that the FDE part meets any requirement regarding missed detection. However the fault detection based on an overall VPL is less strict than the hypothesis test, which should be preferred if additional safety is considered to be given by FDE. A detailed derivation is developed in Appendix A.

III. ARAIM AND PVT INTEGRATION

MHSS utilizes output data that is derived in the PVT estimation. Separate from the geometry and weighting matrices, the pseudorange residuals are used to derive the solution separation d_j. Here, a single bias on one measurement does not show up only in one pseudorange residual, but instead is distributed to all residuals. This results from a dislocation of the user position estimate and user clock offset estimate due to the bias, which in return impacts the pseudorange residuals in the converged all-in-view solution:

$$\begin{aligned}\Delta\mathbf{y} &= (\mathbf{I}-\mathbf{P})\,\mathbf{y} \qquad (24)\\ &= \mathbf{y}-\mathbf{G}\mathbf{S}\mathbf{y}\\ &= \mathbf{y}-\mathbf{G}\hat{\mathbf{x}}\end{aligned}$$

It results from (9) that the partial term in the solution separation results from the set of pseudorange residuals Δy by application of the subset pseudoinverse $\mathbf{S}_j$. With this operation, it is ensured that when computing the partial solution, the entire bias which is distributed over $\Delta\mathbf{y}$ is excluded.

$$\begin{aligned}\Delta x_j &= \mathbf{h}_v\mathbf{S}_j\Delta\mathbf{y} \qquad (25)\\ &= \mathbf{h}_v\mathbf{S}_j\,(\mathbf{I}-\mathbf{G}\mathbf{S}_0)\,\mathbf{y} \qquad (26)\end{aligned}$$

Figure 1 shows how a single bias on PRN E1 distributes into all residuals.

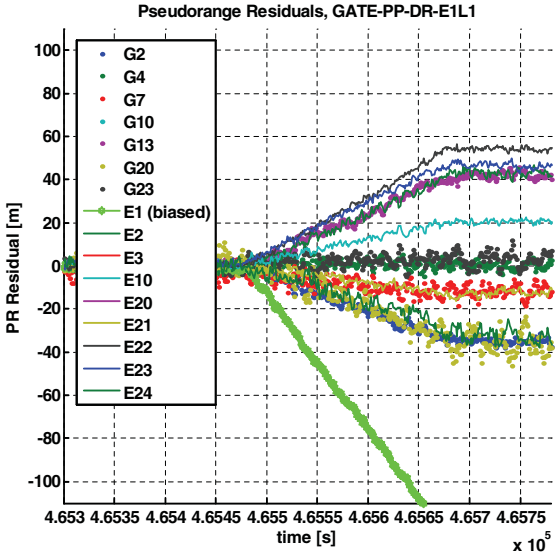

Figure 1. Observed pseudorange residuals with a measurement bias introduced to measurements E1

IV. Demonstration of Integrity in ARAIM Implementation

The following section presents results obtained from Galileo and GPS measurements taken in the GATE Test Environment and using DLR's GALANT receiver. For a nominal scenario and for the case of two simultaneous large measurement biases we show that the ARAIM VPL is robust with respect to the user position error, and that FDE can successfully mitigate the biases.

A. Galileo Test Environment (GATE)

GATE is a Galileo testbed situated in a mountainous area in the south of Germany [12]. It consists of eight transmitter stations (GTS) on mountain peaks surrounding the test area. Although the elevation difference between the core testing area and the transmitter stations is significant, all signals arrive at a relatively small elevation angle compared with satellite-generated GNSS signals.

The test environment supports Virtual Satellite Mode (VSM) where a GPS-based position feedback of the test user and parallel feedback of the received GATE signals into the processing core (GPF) are used to control signal phase and power level. The emitted navigation data corresponds to the measured ranges and imitates a complete space-borne GNSS constellation. Up to eight signals can be simultaneously generated on all Galileo frequencies, where PRN changes are executed under operation.

In addition to the reception of GATE signals, the GPS signal is available in the test area as well. GATE can adapt to the state of the current GPS space segment by using the same Klobuchar parameters that are currently valid for GPS in its error model for the ionospheric delay.

B. Scenarios

Along with multiple interference scenarios [15], [16], the GALANT Receiver was also tested in simulated feared event scenarios especially designed to demonstrate MHSS robustness against large measurement errors on one or multiple satellite ranges. In this paper, we present results from a scenario where two of the eight Galileo signals were affected by pseudorange and carrier phase ramps during the measurement run. Figure 2 shows a graphical representation of the lapse of pseudorange errors. The PRNs were selected such that the impact of the bias on the vertical position error was maximized for the first measurement (E1), and the impact on the horizontal error was maximized for the second PRN (E23). This corresponds to the satellite with highest elevation at the initialization of the error ramp and one satellite with very low elevation.

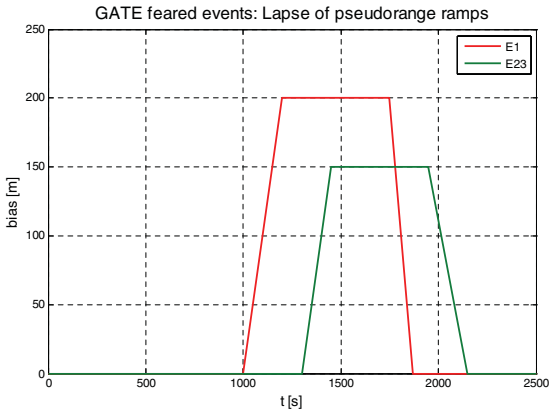

Figure 2. Pseudorange ramps generated on the two Galileo signals for PRNs E1 and E23

The feared event scenarios were recorded simultaneously with two GALANT receivers mounted on the test vehicle, where one receiver was configured to track Galileo measure-

ments on both OS frequencies (E1 and E5), and one receiver recorded Galileo E1 and GPS L1 measurements.

C. GATE measurement error model

For the present work, both the signal types and the method of signal generation produce variability to the properties of the received signals. Satellite signals are generated artificially by being transmitted from mountain peaks, where a dynamic feedback process steers their code and carrier phases, as well as signal power levels. The true direction of arrival does not correspond with the simulated line of sight of the received signals. Thus, elevation dependent modeling of multipath contribution to the measurement error seems unjustifiable. In addition, the E1 and E5 signals use different modulation schemes than traditional GPS signals. Large measurement biases may arise from impreciseness of the measured reference position which is fed back into the processing facility of GATE.

A first basic attempt to model the pseudorange measurement error encountered in this scenario is therefore pursued by analysis of the pseudorange residuals in a fault-free environment. Figure 3 presents an overlay of the pseudorange residuals from both the GPS measurements (dotted) and the Galileo measurements (solid). It can be seen that both groups of observations are only minimally biased compared with the visible measurement noise. In the present analysis, only pseudorange observables have been considered which leads to a higher noise level and limits the applicability of ionosphere-free linear combinations from dual-frequency measurements.

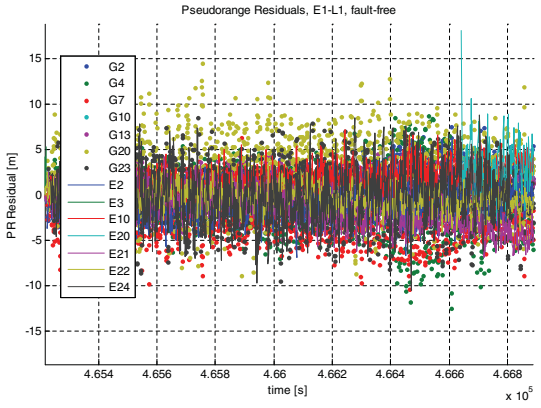

Figure 3. Pseudorange residuals from GATE and GPS measurements, fault free scenario

A histogram of two selected Galileo (GATE) PRNs shows that in fact the distribution of individual residuals seems to consist of a bias term that is quasi-stationary over the duration of the measurement, and a noise contribution which can possibly be approximated by a Gaussian. Significantly more data would be needed however to validate these assumptions.

To guarantee robustness of an MHSS based ARAIM user algorithm, it would be necessary to estimate the measurement

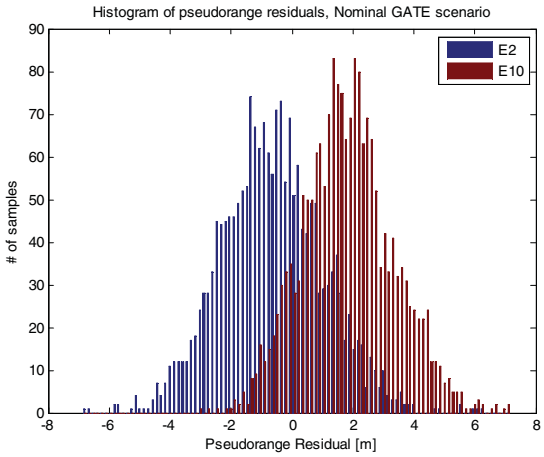

Figure 4. Histogram of two residuals from GATE measurements

error model by a ground network in order to determine maximum Gaussian overbound and maximum bias contributions for the satellites. Using the GATE facilities however does not allow for such long-term observations. The demonstrated capabilities of ARAIM are therefore limited to functional proof, applying an error model that is probably too pessimistic.

D. Fault-free position error and ARAIM VPL

The presented fault free scenarios result from the same set of data that was used for the feared event analysis. To obtain fault-free data, the measurements containing the biases (PRNs E01 and E23) were removed for this analysis.

The 3-D position error obtained from the fault-free scenario suggests that the position estimation algorithm works correctly. A small amount of divergence from the true position can be accounted for imperfectness of the user position feedback that was used to define the GTS signals, and of the lever arm between the GATE user receiver and the GALANT receiver under test. It corresponds well with the biases that can be suspected from Figure 4.

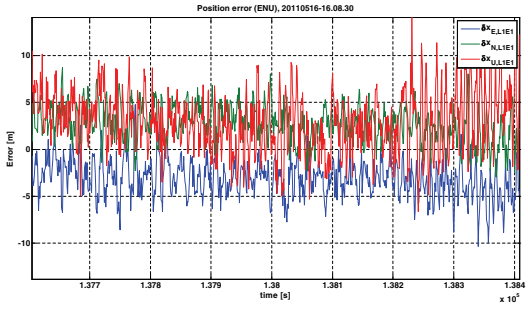

Figure 5. 3-D Position error in nominal scenario, based on Galileo+GPS measurements

The high noise level in the user position estimate can again be explained by the use of code-only measurements.

A combined plot of the magnitude of the vertical position error, the real-time ARAIM VPL and the predicted ARAIM VPL is shown in Figure 6. Two observations can be made: Firstly, the real-time protection level is a rather inexact estimate of the vertical position error, at least for this short measurement interval. This suggests that the nominal error modeling used to describe the Gaussian and bias terms used in the real-time VPL are pessimistic. Those model parameters are URA and $b_{\max}$. Secondly, the prediction of the ARAIM VPL again exceeds the actual measurement-based real-time VPL. This difference is entirely founded in the error model applied to derive D_n, which are URE and b_{nom}.

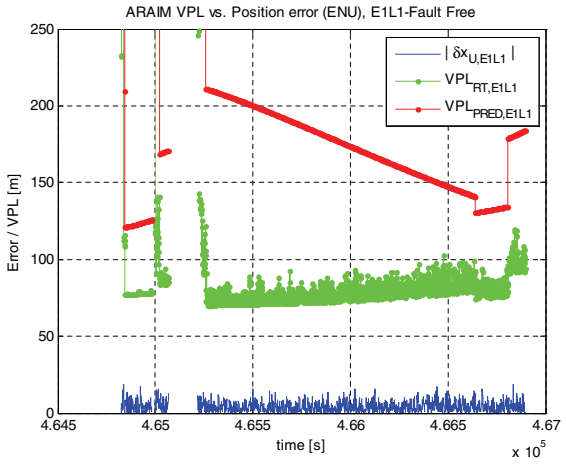

Figure 6. Nominal ARAIM VPL (Real-Time and Prediction)

E. ARAIM under fault conditions

Next, the results from feared event scenarios are presented. In this section, only ARAIM without fault detection is applied, which results in a position solution that uses the all-in-view set of measurements and always contains any bias present in the observations. In Figure 7, the instant when the first pseudorange ramp starts can clearly be estimated both from a slope in the vertical position error (blue) and the real-time VPL (green). Robustness can be guaranteed for this scenario however, because $\forall t : \text{VPL}_{\text{RT}} > |\Delta x|$.

It is worth mentioning that the current GEAS definition for fault detection [7] declines integrity in the interval where $\text{VPL}_{\text{RT}} > \text{VPL}$, which results in a loss of availability. For other types of applications than precision approach, it might however desirable to obtain an error bound with low integrity risk even in the presence of one or more large measurement biases, even if the error bound is very large.

F. Fault Detection with ARAIM

When fault detection and exclusion is applied, the position error can be reduced also in the presence of faults. The following position errors result from processing the same fault scenario with an extended version of ARAIM. The approach uses the $\text{VPL}_{\text{RT}} > \text{VPL}$ test which is a simplified, but less

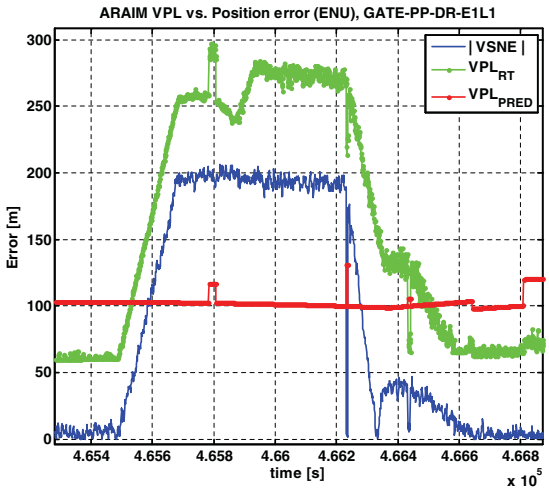

Figure 7. Position error and ARAIM VPLs for the feared event scenario

strict version of the GEAS FD test (see Appendix A). If a fault is detected, the lowest a-priori real-time VPL is determined by sequential computation of ARAIM using measurement subsets. A subset based ARAIM solution is only accepted if it passes the $\text{VPL}_{\text{RT}} > \text{VPL}$ test after exclusion of the satellite. In Figure 8, both FDE-based and MHSS-based protection levels and position errors are jointly shown to allow for a direct comparison.

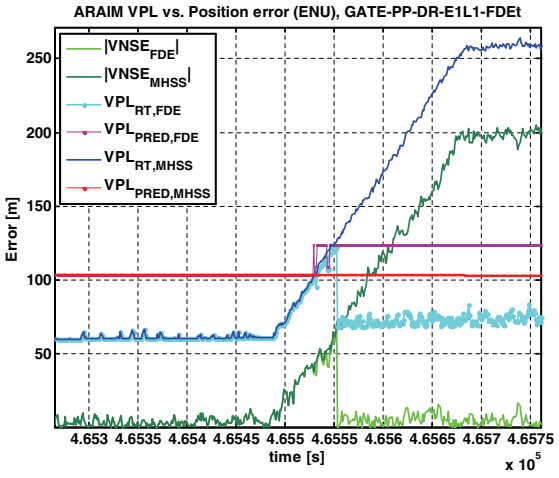

Figure 8. Position error and ARAIM VPLs for the two-faults scenario

It can be observed that after the bias has reached a certain magnitude, the FD test included in the FDE algorithm effects the attempt to exclude a measurement. While the bias is only barely large enough to trigger the test, the exclusion is unsuccessful - the prediction of the FDE VPL is larger due to a reduced geometry, but the position error and the real-time VPL are approximately the same as without FDE. Only after the bias has grown larger, exclusion is successful. The position

error reverts to a nominal level, and the real-time VPL is only slightly larger than before the start of the bias.

V. Conclusions

The presented work demonstrates an implementation of MHSS based ARAIM on a real-time GNSS receiver demonstrator platform. Included in the MHSS approach was a FDE function, where detection of large faults is based on monitoring the partial solutions computed for the ARAIM VPL. The introduction of MHSS and FDE involves a certain extent of additional recursion which may impose limitations to real time use of the algorithm. However in the operational tests in GATE, current state-of-the-art PC hardware was able to process 1Hz data including unconditional FDE recursion in every epoch. Therefore it can be anticipated that future avionics hardware will be able to cope with the computational needs of ARAIM as it is currently envisioned.

Measurement in the GATE testbed were carried out to demonstrate robustness of MHSS-ARAIM and FDE-ARAIM against large measurement faults. Large bias ramps were therefore introduced to the GATE transmitter stations generating two of the Galileo satellite signals while the user receiver was recording data from eight Galileo satellites and the operational GPS signal-in-space.

The MHSS based ARAIM results show that the computed real-time VPL is always robust with respect to the vertical error. However due to the large biases and the selected geometry for the feared event, the vertical error is excessively increased. Introduction of additional FDE can successfully and reliably detect such biases even when multiple faults exist concurrently. With the FDE detection result fed back into position estimation, the navigation error remains small and the performance loss with respect to the vertical error bound VPL is marginal.

Although FDE introduces significant additional complexity to the ARAIM algorithm, it is not necessary to apply it in order to assure integrity robustness in the presence of large faults. Thus, potential limitations caused by implementation constraints for avionics can be encountered by reducing the frequency or depth of the FDE section of ARAIM.

A basic validation of the measurement error model using data samples collected in GATE has been presented. However with limited data available from a single receiver only, the gained observations only allow for a coarse modeling of nominal measurement errors. In the ARAIM results, it can be observed that the margin between the position error and the real time VPL, as well as the margin between real-time VPL and predicted VPL are large. This suggests that the error model is sufficiently conservative and might be adapted towards more optimistic parameters when more data from a ground network becomes available.

Future improvements of the presented real-time concept may include exploiting the capability of using data generated in the PVT and MHSS module to influence interference mitigation, beamforming and tracking modules of the receiver. The availability of DoA information suggests that a joint evaluation of DoA, navigation data and range measurements can improve robustness against threats that are currently not in the scope of conventional MHSS RAIM.

Appendix A
Comparison of Fault Detection and Exclusion Approaches

This section shows that the use of a $\mathrm{VPL}_{\mathrm{RT}} > \mathrm{VPL}$ based fault detection is less conservative than the method proposed in [7], which detects faults at a hypothesis level.

Assuming that the result of ARAIM yields

$$\mathrm{VPL}_{\mathrm{RT}} > \mathrm{VPL} \quad \text{, or} \tag{27}$$

$$\max \mathrm{VPL}_{\mathrm{RT},j} > \max \mathrm{VPL}_j \quad , \tag{28}$$

it follows that there exists one hypothesis where the partial real-time VPL *of this hypothesis* is larger than the overall prediction VPL:

$$\exists j : \mathrm{VPL}_{\mathrm{RT},j} > \mathrm{VPL} \tag{29}$$

From (20) it follows that

$$\forall j : \mathrm{VPL} \geq \mathrm{VPL}_j \quad , \tag{30}$$

and with (29) we have

$$\exists j : \mathrm{VPL}_{\mathrm{RT},j} > \mathrm{VPL}_j \quad . \tag{31}$$

Using (16) and (19) we obtain

$$\exists j : d_j > D_j \quad , \tag{32}$$

and thus, the GEAS-FD test will fail every time the test described in [13] fails. Vice versa, it implies that the GEAS-FD test is more strict than the $\mathrm{VPL}_{\mathrm{RT}} > \mathrm{VPL}$ based test and should be preferred.

Acknowledgment

The author wishes to express his gratitude to all his colleagues involved in the GALANT project, who did a great job in putting together an experimental GNSS receiver platform and also put lots of effort into preparation and conduction of the measurement campaign at GATE. My special thanks goes to Dr. Andriy Konovaltsev and Carsten Becker who were superior partners in integrating the receiver-side software with the PVT and Integrity module.

Furthermore the author would like to thank Dr. Juan Blanch from Stanford University for his continuing readiness to discuss aspects ARAIM implementations, the underlying assumptions and the framework for multiple constellation RAIM in general.

Last, I would like to thank my colleagues Dr. Alexandru Spletter who has given me a lot of opportunity to work on novel FDE techniques for ARAIM, and Boubeker Belabbas who is a reliable discussion partner, scientific advisor and group leader.

REFERENCES

[1] A. Ene, J. Blanch, and T. Walter, "Galileo-GPS RAIM for Vertical Guidance," in *Proceedings of the Institute of Navigation's National Technical Meeting, Monterey CA*, 2006.

[2] J. Blanch, A. Ene, T. Walter, and P. Enge, "An Optimized Multiple Hypothesis RAIM Algorithm for Vertical Guidance," in *Proceedings of the ION GNSS 2007 Conference*, 2007.

[3] B. S. Pervan, S. P. Pullen, and J. R. Christie, "A Multiple Hypothesis Approach to Satellite Navigation Integrity," *Journal of The Institute of Navigation*, vol. 45, no. 1, 1998.

[4] T. Walter and P. Enge, "Weighted RAIM for Precision Approach," in *Proceedings of the ION GNSS Conference 1995*. ION, 1995. [Online]. Available: http://waas.stanford.edu/~wwu/papers/gps/PDF/wraim_tfw95.pdf

[5] M. Rippl, A. Spletter, and C. Günther, "Parametric Performance Study of Advanced Receiver Autonomous Integrity Monitoring (ARAIM) for Combined GNSS Constellations," in *Proceedings of the 2011 International Technical Meeting of the Institue of Navigation (ITM2011)*.

[6] FAA GEAS Panel, "GNSS Evolutionary Architecture Study: Phase I - Panel Report," Feb. 2008. [Online]. Available: http://www.faa.gov/about/office_org/headquarters_offices/ato/service_units/techops/navservices/gnss/library/documents/media/GEAS_PhaseI_report_FINAL_15Feb08.pdf

[7] ——, "Phase II of the GNSS Evolutionary Architecture Study," Feb. 2010. [Online]. Available: http://www.faa.gov/about/office_org/headquarters_offices/ato/service_units/techops/navservices/gnss/library/documents/media/GEASPhaseII_Final.pdf

[8] S. Jan, W. Chan, T. Walter, and P. Enge, "Matlab Simulation Toolset for SBAS Availability Analysis," in *Proceedings of the ION GNSS Conference 2001*, 2001.

[9] A. Ene, "Utilization of Modernized Global Navigation Satellite Systems for Aircraft-Based Navigation Integrity," Ph.D. dissertation, Stanford University, Jun. 2009.

[10] M. Choi, J. Blanch, T. Walter, and P. Enge, "Advanced RAIM Demonstration Using Four Months of Ground Data," in *Proceedings of the International Technical Meeting of the Institue of Navigation (ITM2011)*, 2011.

[11] M. Choi, J. Blanch, D. Akos, L. Heng, G. Gao, T. Walter, , and P. Enge, "Demonstrations of Multi-constellation Advanced RAIM for Vertical Guidance Using GPS and GLONASS Signals," in *Proceedings of the 24th International Technical Meeting of the Satellite Division of The Institue of Navigatoin - ION GNSS*, 2011.

[12] Website of the GATE testbed. [Online]. Available: http://www.gate-testbed.com/

[13] A. Spletter and M. Rippl, "Novel Satellite Fault Isolation Method for Real-Time Advanced RAIM Algorithms," in *Proceedings of the 24th International Technical Meeting of the Satellite Division of The Institue of Navigatoin - ION GNSS*, 2011.

[14] DLR Institute of Communications and Navigation (IKN). (2012) GALANT - Galileo Antenna Demonstrator. [Online]. Available: http://www.dlr.de/kn/en/desktopdefault.aspx/tabid-4306/6938_read-9224/

[15] M. Cuntz, A. Konovaltsev, M. Sgammini, C. Hättich, G. Kappen, M. Meurer, A. Hornbostel, and A. Dreher, "Field Test: Jamming the DLR Adaptive Antenna Receiver," in *Proceedings of the 24th International Technical Meeting of the Satellite Division of The Institue of Navigatoin - ION GNSS*, 2011.

[16] C. Hättich, M. Cuntz, A. Konovaltsev, G. Kappen, and M. Meurer, "Robust Multi-Antenna Acquisition in Time, Frequency and Space for a Digital Beamforming Receiver," in *Proceedings of the 24th International Technical Meeting of the Satellite Division of The Institue of Navigatoin - ION GNSS*, 2011.

[17] M. Cuntz, H. Denks, A. Konovaltsev, A. Hornbostel, A. Dreher, and M. Meurer, "GALANT - Architecture Design and First Results of a Novel Galileo Navigation Receiver Demonstrator with Array Antennas," in *Proceedings of the ION GNSS Conference*, 2008.

[18] A. Ene, "Multiple Hypothesis RAIM with Real-Time FDE and Forecasted Availability for Combined Galileo-GPS Vertical Guidance," vol. Proceedings of the European Navigation Converence - GNSS/TimeNav, May 2007.

[19] J. Blanch, T. Walter, and P. Enge, "RAIM with Optimal Integrity and Continuity Allocations Under Multiple Failures," *IEEE Transactions on Aerospace and Electronic Systems*, vol. 46, no. 3, pp. 1235–1247, Jul. 2010.

[20] International Civil Aviation Organization (ICAO), *Annex 10, Aeronautical Telecommunications, Volume I (Radio Navigation Aids)*, Std., 2005.

[21] J. Blanch and T. Walter, "LPV-200 Requirements Interpretation, draft paper," 8. November 2011.